Three-Dimensional Planar Radiating Structures in Stratified Media

Philippe Gay-Balmaz, Juan R. Mosig

Laboratoire d'Electromagnétisme et d'Acoustique, Ecole Polytechnique Fédérale de Lausanne, CH-1015 Lausanne, Switzerland

Received 11 December 1995; revised 12 July 1996

ABSTRACT: This article presents new developments concerning three-dimensional (3-D) planar problems, that is, combinations of planar sheets of current oriented along normal and transverse directions in a stratified medium. The conducting structures are analyzed using an improved version of the mixed potential integral equation, including unknown currents along three coordinate directions, and solved through a method of moments. The modifications needed in the integral equation to accommodate simultaneously normal and transverse currents are discussed. Detailed expressions for the Green's functions associated with horizontal and vertical dipoles are presented and cast as Sommerfeld integrals. A convenient integration path is proposed for their estimation. Associated interpolation problems are thoroughly discussed and symmetry and reciprocity considerations are pointed out. Finally, two antennas have been built and studied to demonstrate the validity of the formulation: a short-circuited microstrip antenna, and a two-layer patch antenna. © 1997 John Wiley & Sons, Inc. *Int J Microwave Millimeter-Wave CAE* **7: 330–343, 1997.**

Keywords: mixed-potential integral equation; multidimensional interpolations; vertical metallizations; microstrip antenna

INTRODUCTION

Classical microstrip antennas are usually modeled as two-dimensional (2-D) structures when using integral equation theory. However, even a simple structure like the coax-fed microstrip patch already contains vertical currents arising in the coaxial feed pin. Vertical currents are also present in other practical structures like shielded microstrip subarrays [1] where vertical wires are used to suppress parasitic surface wave modes. Traditionally, the difficulty of dealing with vertical currents is removed by introducing a simplified model where the coax pin appears as a point excited in the patch, from where the current flows outwards [2, 3]. But, to rigorously analyze coax-fed patches, we need to consider a three-dimensional (3-D) planar metallic object, therefore including three current components embedded in a stratified medium. The same problem arises when dealing with more complex structures like short-circuited antennas, interconnected stacked patches, via-hole devices, or plates whose thicknesses cannot be neglected when compared with the wavelength. This article provides the theoretical foundation needed to apply the *mixed potential integral equation* (MPIE) to 3-D planar metallic bodies embedded in a layered medium, and presents some useful examples.

The MPIE has been used to solve 2-D structures embedded in multilayered substrates [3, 4]. This method proved to be very efficient and has been widely adopted when the integral equation is solved in the space domain [5, 6]. Later on, the MPIE had been extended to provide a rigorous analysis of coax-fed microstrip patches [7, 8], but the proposed model was too specifically linked to

Correspondence to: P. Gay-Balmaz
Contract grant sponsor: European Community
Contract grant number: COST-245

 CCC 1050-1827/97/050330-14

that particular geometry and could not be easily generalized. The needed general theory has been presented in ref. [9 and 10], where the problem of an arbitrary metallic scatterer embedded in a flat layered medium is presented, and a far-reaching discussion of the possible MPIE versions for this geometry is provided.

Other methods, different from MPIE, have been used recently to study antennas including vertical metallizations; for instance, in ref. 11, the analysis of *planar inverted-F antennas* (PIFA), commonly used in mobile radio communication, was done with the *spatial network method* (SNM). Another example [12] is the analysis of a printed circular patch antenna with a central cylindrical conductor enhancing the bandwidth, using a cavity model. In another study [13], a microstrip antenna including a ground wire which connects the patch to the ground plane was presented; the investigators used a *finite difference time domain* method (FDTD) and found a resonance frequency below the classical cavity resonance modes. Within the same framework, a microstrip air-bridge has also been studied [14] using a *spectral domain approach* (SDA) and partial Galerkin solutions. A more theoretical development associated with vertical metallizations was proposed in ref. 15, again using a SDA; the example of an air-bridge is presented.

In the present study, all steps for solving a 3-D planar problem with the help of the MPIE and the *method of moments* (MoM) are investigated. First, the MPIE is introduced in the next section, where the traditional choice for Green's functions is recalled. Then the problem of the multiple choice for the scalar potential is discussed in the subsequent section and a convenient choice is made thereafter. Then, the spatial domain representation is recovered using Sommerfeld integrals. The traditional integration path for Sommerfeld integrals is the real axis of the complex spectral plane. Here, to avoid singularities, a portion of the real axis is deformed into an elliptic path well inside the complex plane. The tail contribution over the real axis is evaluated using the *weighted averages algorithm* [4]. An original feature of the technique presented in this article is the 3-D interpolation procedure, which requires a more detailed study of the Green's functions. In particular, the dependence of the (z-) coordinates must be well known. Also, the symmetrical character of the Green's functions is studied to determine symmetries for reducing the CPU time. The MoM implementation requires special basis functions at the bends and edges of the structure, which can be formed where horizontal and vertical metallic surfaces do intersect. The article concludes with the study of two practical multilayered antennas, including bends and edges.

MPIE AND VECTOR POTENTIAL DYADIC GREEN'S FUNCTION

Figure 1 depicts a generic example of the type of structure to consider in this article. These structures can be analyzed by using the E-field boundary condition:

$$\mathbf{n} \times (\mathbf{E}^e + \mathbf{E}^s) = Z_s \mathbf{J}_s \tag{1}$$

with:

$$\mathbf{E}^s(\mathbf{r}) = \int_S \overline{\overline{\mathbf{G}}}_{EJ}(\mathbf{r} \mid \mathbf{r}') \cdot \mathbf{J}_s(\mathbf{r}')\, ds' \tag{2}$$

This equation is simply a Leontovich boundary condition expressing that the total tangential field on conducting surfaces is proportional to the surface current. Here, $\mathbf{E}^e$ is an excitation field, $\mathbf{E}^s$ the scattered field, $\mathbf{n}$ is the unit vector normal to the conducting surfaces, S is the union of all the conducting surfaces, and Z_s is an effective surface impedance (ohm/square) providing a first-order treatment of lossy conductors. As a practical rule, skin effect impedance values may be used for Z_s, although determining the correct value of Z_s is a complex problem in the case of very thin conductors ideally modeled by current sheets [16]. In the absence of magnetic currents, the scattered electric field can be always written in terms of potentials as:

$$\mathbf{E}^s = -j\omega\mathbf{A} - \nabla V \tag{3}$$

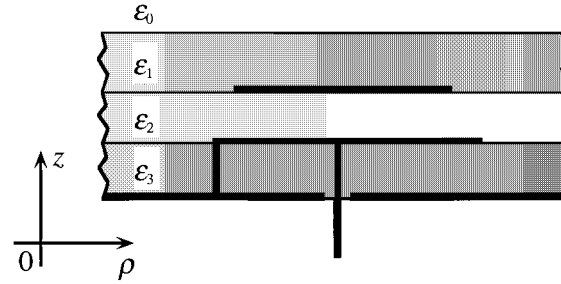

Figure 1. The general 3-D planar structure considered in this work.

The question is now whether we can generalize the conventional expressions:

$$\mathbf{A}(\mathbf{r}) = \int_S \overline{\overline{\mathbf{G}}}_A(\mathbf{r} \mid \mathbf{r}') \cdot \mathbf{J}_s(\mathbf{r}')\, ds'$$

$$V(\mathbf{r}) = \int_S G_V(\mathbf{r} \mid \mathbf{r}') q_s(\mathbf{r}')\, ds' \tag{4}$$

where $q_s = -\nabla' \cdot \mathbf{J}_s / j\omega$, to a 3-D conducting structure embedded in a layered medium, and which are the pertinent values of the Green's functions, $\overline{\overline{\mathbf{G}}}_A$ and G_V. We will then obtain the traditional formulation of the MPIE:

$$-\mathbf{n} \times \mathbf{E}^e(\mathbf{r}) = \mathbf{n} \times \left[-j\omega \int_S \overline{\overline{\mathbf{G}}}_A(\mathbf{r}|\mathbf{r}') \cdot \mathbf{J}_s(\mathbf{r}')\, ds' + \frac{1}{j\omega} \nabla \int_S G_V(\mathbf{r}|\mathbf{r}') \nabla' \cdot \mathbf{J}_s(\mathbf{r}')\, ds' \right] - Z_m \mathbf{n} \times \mathbf{J}_s(\mathbf{r}) \tag{5}$$

In the case of purely horizontal currents, $\mathbf{J} = (J_s, J_y, 0)$, or purely vertical ones, $\mathbf{J} = (0, 0, J_z)$, the problem has been traditionally solved by following the so-called Sommerfeld choice for $\overline{\overline{\mathbf{G}}}_A$ [3, 7, 17]. If we tentatively collect these results in a unique dyadic, we obtain the formal Sommerfeld representation:

$$\overline{\overline{\mathbf{G}}}_A = \begin{bmatrix} G_A^{xx} & 0 & 0 \\ 0 & G_A^{yy} & 0 \\ G_A^{zx} & G_A^{zy} & G_A^{zz} \end{bmatrix} \tag{6}$$

Specific values of the dyadic components depend, of course, on the geometry of the layered medium. They are traditionally calculated by working in the spectral domain, thanks to the Fourier transform pair:

$$\tilde{f}(k_x, k_y) = \frac{1}{2\pi} \int_{-\infty}^{\infty} \int_{-\infty}^{\infty} f(x, y) \exp(-jk_x x) \times \exp(-jk_y y)\, dx\, dy \tag{7a}$$

$$f(x, y) = \frac{1}{2\pi} \int_{-\infty}^{\infty} \int_{-\infty}^{\infty} \tilde{f}(k_x, k_y) \exp(jk_x x) \times \exp(jk_y y)\, dk_x\, dk_y \tag{7b}$$

Now, in the spectral domain, it is always possible to obtain analytical values of the normal components of the dyadic Green's function for the fields $\tilde{G}_{EJ}^{zs}, \tilde{G}_{HJ}^{zs}$, where $s = x, y, z$. Then, $\tilde{G}_A^{st}$ components can be expressed in terms of these quantities and their normal derivatives ($\partial f / \partial z = \dot{f}$) as [4, 7]:

$$\overline{\overline{\tilde{\mathbf{G}}}}_A = \begin{bmatrix} -\dfrac{\mu \tilde{G}_H^{zx}}{jk_y} & 0 & 0 \\ 0 & \dfrac{\mu \tilde{G}_H^{zy}}{jk_x} & 0 \\ \dfrac{\mu(k_x/k_y)\dot{\tilde{G}}_H^{zx} + j\omega\varepsilon\mu \tilde{G}_E^{zx}}{k_\rho^2} & \dfrac{-\mu(k_y/k_x)\dot{\tilde{G}}_H^{zy} + j\omega\varepsilon\mu \tilde{G}_E^{zy}}{k_\rho^2} & \dfrac{j\omega\varepsilon\mu \tilde{G}_E^{zz}}{k_\rho^2} \end{bmatrix} \tag{8}$$

with $k_\rho = \sqrt{k_x^2 + k_y^2}$ and where, for the sake of simplicity, we restrain ourselves to the nonsingular case $\mathbf{r} \neq \mathbf{r}'$. Now, it is well known [4, 9, 10, 19] that the choice (6, 8) for $\overline{\overline{\mathbf{G}}}_A$ leads to a nonunique value of the scalar Green's function, G_V. While this is not a hindrance in problems dealing exclusively with either purely horizontal or purely vertical currents, the multiple definition of G_V must be seriously considered in geometries like the one depicted in Figure 1, including bends and edges where the current shifts abruptly between horizontal and vertical directions.

POSSIBLE CHOICES FOR SCALAR POTENTIAL GREEN'S FUNCTIONS

As we know, the vector and the scalar potentials are related by the Lorentz gauge:

$$\nabla \cdot \mathbf{A} + j\omega\varepsilon\mu V = 0 \tag{9}$$

When applied to the potentials of an unit u-directed Hertz dipole, the Lorentz gauge gives [14]:

$$\nabla \cdot \left(\overline{\overline{\mathbf{G}}}_A \cdot \hat{\mathbf{e}}_u \right) + j\omega\varepsilon\mu \left(\frac{1}{j\omega} \frac{\partial G_V}{\partial u'} \right) = 0 \quad (10)$$

where $\hat{\mathbf{e}}_u$ indicates an arbitrary direction of the source dipole *XED*, *YED*, or *ZED* ($u = x, y, z$). It is worth point out that the scalar potential, V, in the generic equation [eq. (9)] does not become G_V in the specific application [eq. (10)], but rather the scalar potential of two point charges associated with the dipole by the continuity equation. Now, eq. (10) may be viewed as a practical way of defining and computing G_V in the spectral domain. Unfortunately, when introducing eq. (8) into eq. (10), we get two different values for G_V, which we will call transverse and normal (G_V^t, G_V^n). If $u = x, y$, we obtain $G_V^{(XED)} = G_V^{(YED)} = G_V^t$ and:

$$\frac{\partial}{\partial u'} G_V^t = -\frac{1}{\varepsilon\mu} \left(\nabla \cdot \overline{\overline{\mathbf{G}}}_A \right) \cdot \hat{\mathbf{e}}_u \quad u = x, y \quad (11)$$

whose solution in the spectral domain is:

$$\begin{aligned} \tilde{G}_V^t &= \frac{j\omega}{jk_x k_\rho^2} \dot{\tilde{G}}_E^{zx} - \frac{k^2}{\varepsilon j k_y k_\rho^2} \tilde{G}_H^{zx} \\ &= \frac{j\omega}{jk_y k_\rho^2} \dot{\tilde{G}}_E^{zy} + \frac{k^2}{\varepsilon j k_x k_\rho^2} \tilde{G}_H^{zy} \end{aligned} \quad (12)$$

whereas $u = z$ leads to $G_V^{(ZED)} = G_V^n$ with:

$$\frac{\partial}{\partial z'} G_V^n = -\frac{1}{\varepsilon\mu} \left(\nabla \cdot \overline{\overline{\mathbf{G}}}_A \right) \cdot \hat{\mathbf{e}}_z \quad (13)$$

and finally:

$$\tilde{G}_V^n = -\frac{j\omega}{k_\rho^2} \int \dot{\tilde{G}}_E^{zz} \, dz' \quad (14)$$

SELECTING A COUPLE OF GREEN'S FUNCTIONS FOR SCALAR AND VECTOR POTENTIALS

Classical electromagnetic theory [9] tells us that a couple of potentials, $\mathbf{A}, V$ may be replaced by $\mathbf{A} - \nabla\psi$ and $V + \psi$ without affecting the fields. In terms of Green's functions, this means that we should be able to modify the two first columns of $\overline{\overline{\mathbf{G}}}_A$ to arrive at a unique scalar Green's function, G_V^n, or to modify the last column of $\overline{\overline{\mathbf{G}}}_A$ to obtain G_V^t as unique solution. This point has been discussed in ref. 9. Here, we follow the choice $G_V = G_V^t$ and we introduce a new dyadic $\overline{\overline{\Gamma}}_A$ for the vector potential, having the two first columns identical to $\overline{\overline{\mathbf{G}}}_A$:

$$\frac{\partial}{\partial u'} G_V^t = -\frac{1}{\varepsilon\mu} \left(\nabla \cdot \overline{\overline{\Gamma}}_A \right) \cdot \hat{\mathbf{e}}_u \quad u = x, y \quad (15)$$

but we modify the third column to fulfill the following equation:

$$\frac{\partial}{\partial z'} G_V^t = -\frac{1}{\varepsilon\mu} \left(\nabla \cdot \overline{\overline{\Gamma}}_A \right) \cdot \hat{\mathbf{e}}_z \quad (16)$$

Taking the gradient of the difference between eqs. (16) and (13) we obtain:

$$\begin{aligned} \Gamma_A^{uz} &= G_A^{uz} + \frac{1}{\omega^2} \frac{\partial}{\partial u \, \partial z'} (G_V^t - G_V^n); \\ & u = x, y, z \end{aligned} \quad (17)$$

This equation fully defines the new dyadic Green's function to be used in combination with G_V^t for arbitrary current distributions. Therefore, the scattered field in eq. (3) derives from the following potentials:

$$\begin{aligned} \mathbf{A}(\mathbf{r}) &= \int_S \overline{\overline{\Gamma}}_A(\mathbf{r} \mid \mathbf{r}') \cdot \mathbf{J}_s(\mathbf{r}') \, ds' \\ V(\mathbf{r}) &= \int_S G_V^t(\mathbf{r} \mid \mathbf{r}') q_s(\mathbf{r}') \, ds' \end{aligned} \quad (18)$$

Michalski [9] has proposed to absorb in the scalar potential the new components [eq. (17)] of the dyadic $\overline{\overline{\Gamma}}_A$ with the result:

$$\begin{cases} \mathbf{A}(\mathbf{r} \mid \mathbf{r}') = \displaystyle\int_S \overline{\overline{\mathbf{G}}}_A(\mathbf{r}) \cdot \mathbf{J}_s(\mathbf{r}') \, ds' \\ V(\mathbf{r} \mid \mathbf{r}') = \displaystyle\int_S G_V^t(\mathbf{r}) q_s(\mathbf{r}') \, ds' \\ \quad + \displaystyle\int_S \frac{1}{j\omega} \frac{\partial}{\partial z'} (G_V^n(\mathbf{r} \mid \mathbf{r}') \\ \quad - G_V^t(\mathbf{r} \mid \mathbf{r}')) J_{sz}(\mathbf{r}') \, ds' \end{cases} \quad (19)$$

which demonstrates that we can keep using the original Sommerfeld choice, $\overline{\overline{\mathbf{G}}}_A$, if we correct the scalar potential with a term proportional to the normal component of the current.

INTEGRATION IN THE COMPLEX PLANE

Expressions for the Green's functions associated with the potentials have been given in the spectral domain in the second and third sections. Now, the space domain must be recovered by performing the *inverse Fourier transform* [eq. (7b)]. It can be shown [4] that, for potentials, the double Fourier transform can be reduced to a combination of Hankel transforms:

$$\tilde{f}(k_\rho) = \int_0^\infty J_0(k_\rho \rho) f(\rho) \rho \, d\rho \qquad (20a)$$

$$f(\rho) = \int_0^\infty J_0(k_\rho \rho) \tilde{f}(k_\rho) k_\rho \, dk_\rho \qquad (20b)$$

with $\rho = \sqrt{x^2 + y^2}$ and $k_\rho = \sqrt{k_x^2 + k_y^2}$.

Usually, the integration path has been taken by most investigators as the real axis of the complex plane, k_ρ, in which case there is no need to evaluate Bessel functions of complex arguments. The success of such a strategy depends strongly on an accurate localization of the existing poles (surface waves) and on the subsequent evaluation of the residues. This task is easily done for a single thin layer, but unfortunately, becomes very time-consuming in the presence of thick or multilayered substrates. Therefore, an integration path that avoids all the poles and eliminates the need to search for them is chosen here. It can be shown that the behavior of the Green's function is essentially oscillating along the real axis with poles between $k_0 < k_\rho < k_0\sqrt{\max(\varepsilon_r \mu_r)}$ for a lossless structure, and exponential along the imaginary axis. Figure 2 shows the behavior in the complex plane k_ρ of the modulus of the complex function to be integrated for the evaluation of $G_V^{(XED)}$ for a single-layer microstrip structure. The ideal path should go through the saddle point and then back to the real axis beyond $k_\rho = k_0\sqrt{\varepsilon_{r1}}$. In practice, many numerical simulations have shown that the choice of the path is not critical. An ellipse having its center at $k_\rho = k_0(1 + \sqrt{\varepsilon_{r\,\max}})/2$ and its semi-axis, which is parallel to the imaginary axis, inversely proportional to ρ, may be considered a good choice. This path avoids numerical problems due to the exponential behavior of the Bessel functions when the imaginary part of its argument grows. Other paths are possible [20–22] but an ellipse was selected because of its flexibility and simplicity (no need to break into segments). Figure 3 illustrates the choice of the integration path. For the numerical integration, the semiellipse is parameterized in the usual way and a standard Gaussian quadrature is applied. The total number of integration points should, of course, grow with the value of the radial source–observer distance ρ to keep a fixed accuracy. On the other hand, the complexity of the algorithm is independent of the number of layers and of their physical and electrical characteristics. Finally, the integration over the real axis is performed using the efficient *weighted-averages algorithm* [4].

INTERPOLATIONS

In spite of the rather sophisticated treatment presented in the previous sections, the computation of a Green's function through the evaluation of a Sommerfeld integral remains a time-consuming process. Therefore, it is not realistic to compute a new Sommerfeld integral every time a Green's function value is required. One of the most common solutions in the past has been to perform interpolation on a set of precalculated integrals [3, 23]. Interpolation is particularly necessary in a 3-D planar problem, where Green's functions can be a function of up to three coordinates ρ, z, z'. In fact, even for a relatively simple 3-D planar structure (such as the short-circuited microstrip antenna presented in Fig. 4a), three cases must already be considered. One-dimensional interpolation is sufficient when the interactions between the source and the observation points depend only on the radial horizontal distance (Fig. 4b). On the other hand, two-dimensional interpolation is necessary if the interactions depend additionally on the height of the source or on the height of the observer (Fig. 4c and d). Finally, in the worst case, one needs a three-dimensional interpolation. This happens when the interactions depend on the radial horizontal source–observer distance and also on the position of the source and of the observer above the ground (Fig. 4e). In cases where interpolation is done on the normal (z-) coordinates (2-D or 3-D), a small number of horizontal planes (values of z) must be selected to tabulate the corresponding integrals. The choice of these planes depends on the behavior of the Green's functions at the ground plane and at the interfaces. If the ground plane is modeled by a perfect electric conductor, some Green's functions vanish on it and need not to be computed. Also, for a successful interpola-

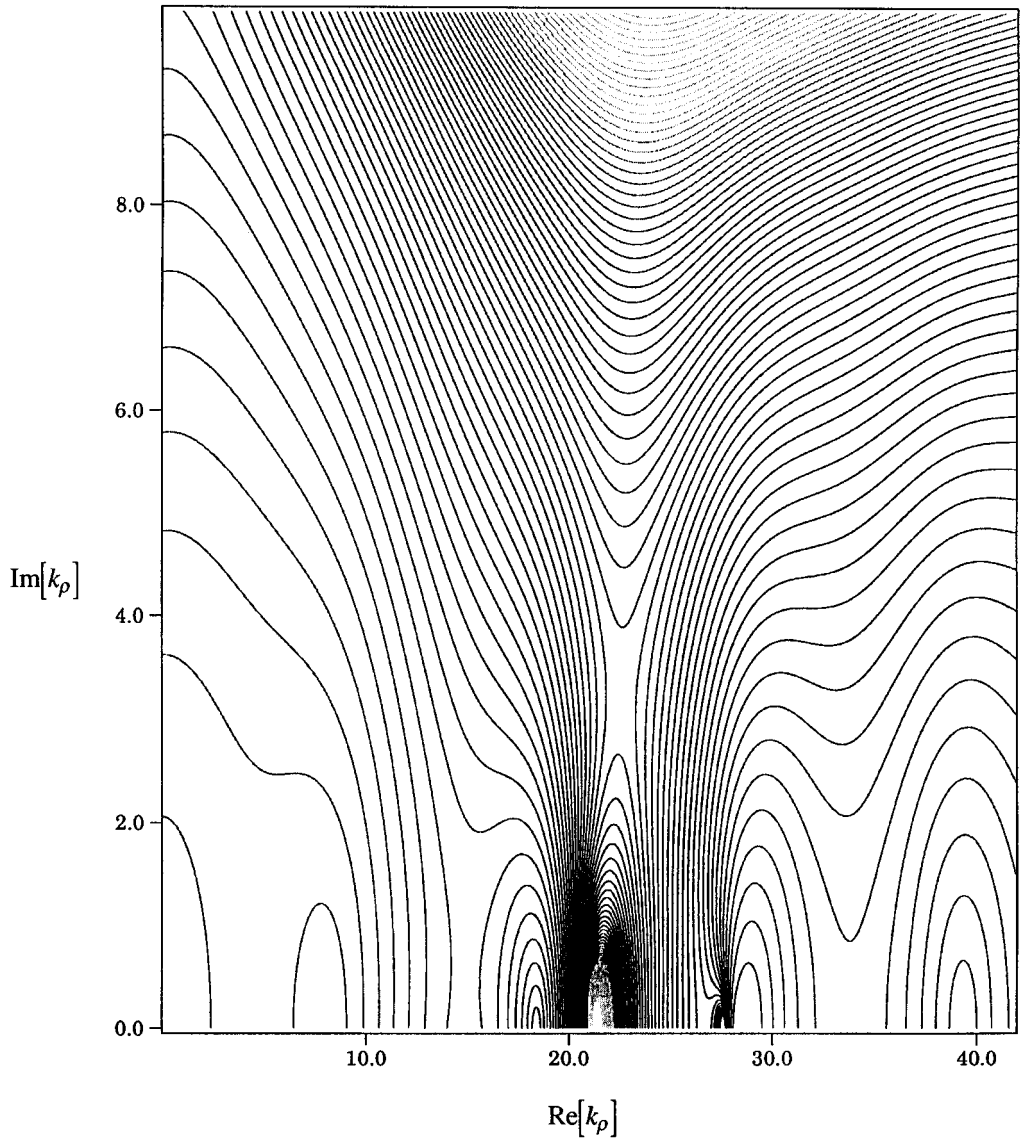

Figure 2. Behavior of $J_0(k_\rho \rho) \cdot \tilde{G}_V^{(XED)}$ in the complex k_ρ plane for a single-layer microstrip structure. The frequency is 1 GHz ($k_0 = 20\pi/3$). The substrate has a thickness of 0.01 λ and a relative permittivity of 4. The radial source–observer distance, ρ, is 1 λ.

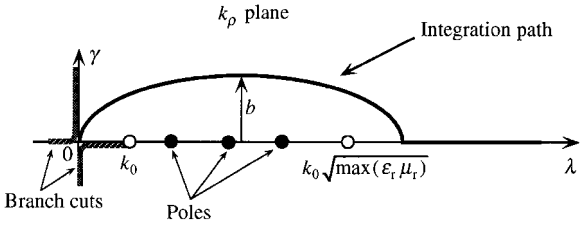

Figure 3. Integration path used in the Sommerfeld integrals.

tion, the different behaviors of the Green's functions must be clearly understood. If the function and its derivative are both continuous at an interface, the choice of the interpolating points is not constrained by the interfaces and the simplest choice is to select a small number of equidistant points (Fig. 5a). Whenever the Green's function is continuous, but its derivative is not, a point must be picked up at the interface (Fig. 5b), whereas, in the worst case (discontinuous function), two points, one just above and one just below the interface, are selected (Fig. 5c). The next section

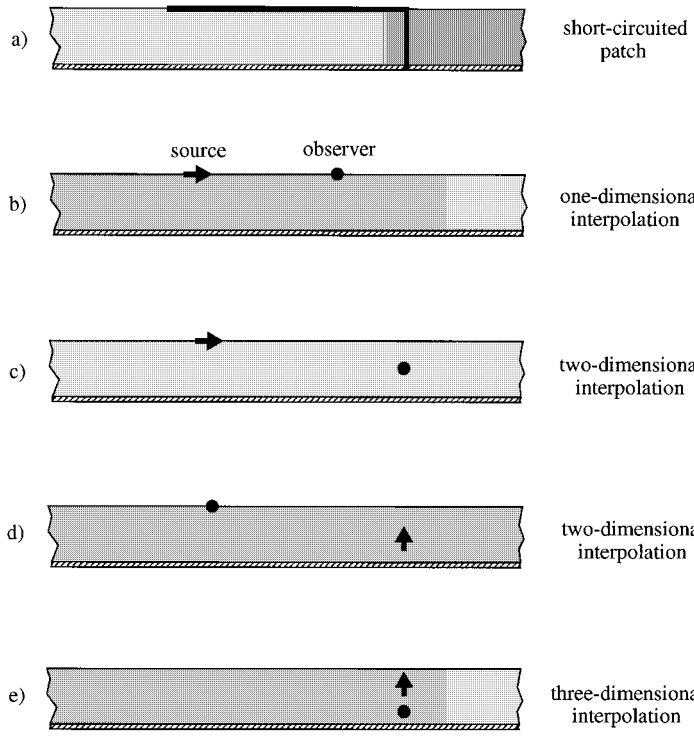

Figure 4. Different possibilities for interpolations.

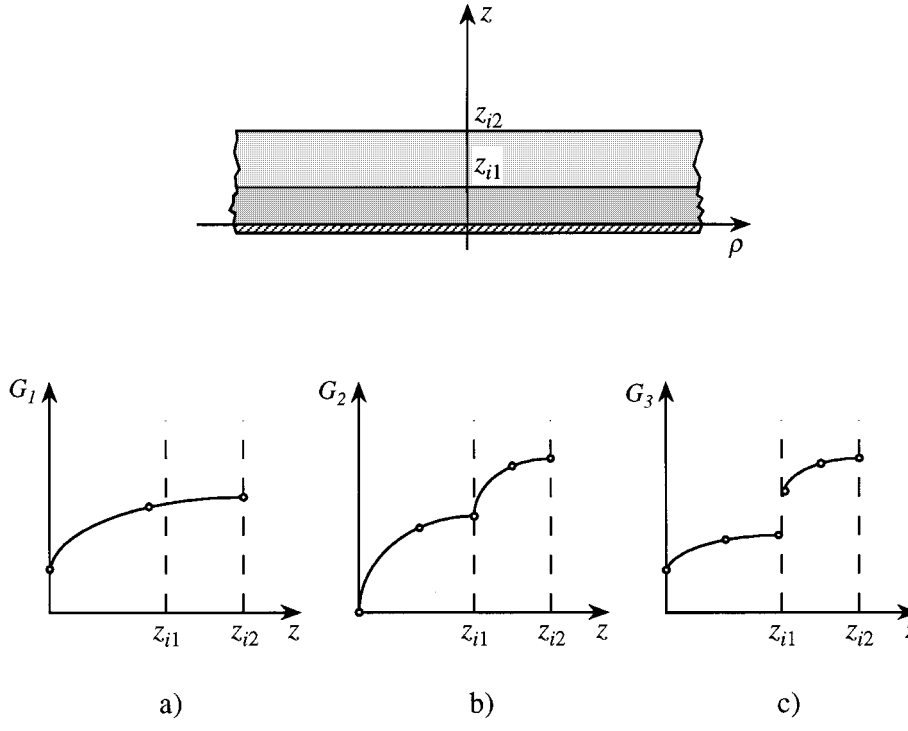

Figure 5. Choices for interpolation points.

discusses the different behaviors observed for the Green's functions.

PROPERTIES OF GREEN'S FUNCTIONS

Because, in our type of problem, Green's functions may refer to observers and sources at variable heights, the interpolations in the vertical plane concern the unprimed coordinate z as well as the primed coordinate z'. Therefore, the behavior of the Green's functions associated with the potentials must be studied when the observer point reaches the ground plane or crosses an interface *and* the same must be done for the source point. The needed information is obtained by a careful inspection of the *boundary conditions* combined with the *reciprocity theorem*. We will just summarize the final conclusions concerning the continuity and the behavior on the ground plane of the Green's functions:

1. For an observer reaching the ground plane:

$$G_A^{xx} = G_V^{(XED)} = G_V^{(ZED)} = 0$$
$$G_A^{zx} \text{ and } G_A^{zz} \neq 0 \qquad (21)$$

2. For a source point reaching the ground plane:

$$G_A^{xx} = G_A^{zx} = G_A^{(XED)} = G_V^{(ZED)} = 0$$
$$G_A^{zz} \neq 0 \qquad (22)$$

3. For an observer crossing an interface:

$$G_A^{xx}, G_V^{(XED)}, G_V^{(ZED)} \text{ are continuous}$$
$$G_A^{zx} \text{ and } G_A^{zz} \text{ are discontinuous} \qquad (23)$$

   Note that G_A^{zx} and G_A^{zz} are discontinuous only in cases where the permeabilities of the two media are different.

4. For a source point crossing an interface:

$$G_A^{xx}, G_A^{zx}, G_V^{(XED)} \text{ are continuous}$$
$$G_V^{(ZED)} \text{ and } G_A^{zz} \text{ are discontinuous} \qquad (24)$$

As for the continuity of derivatives, it can be shown that all the derivatives with respect to z of the potential functions are discontinuous. A simple and practical way to check these results is to evaluate numerically the Green's functions of a single-layer microstrip for a fixed radial distance ρ as a function of vertical coordinates z, z'.

Another crucial step to reduce the number of calculations is to determine, with the help of the *reciprocity theorem*, which Green's functions obey the following symmetry property: $G(\mathbf{r}, \mathbf{r}') = G(\mathbf{r}', \mathbf{r})$. Many computations can be avoided using this property. For N horizontal interpolating planes, the symmetry property just defined allows reduction of the number of cases to be computed from N^2 to $N(N-1)/2$. The translational property applied to any dyadic Green's function defined in a planar layered medium can be written as [4]:

$$G(\mathbf{r} \mid \mathbf{r}') = G(x, y, z|x', y', z') = G(x - x', y - y', z \mid 0, 0, z') \qquad (25)$$

Therefore, if the Fourier transform of $G(\mathbf{r} \mid \mathbf{r}')$ is $\tilde{G}(k_x, k_y, z|z')$, the Fourier transform of $G(\mathbf{r}' \mid \mathbf{r})$ is defined by $\tilde{G}(-k_x, -k_y, z'|z)$. In the spectral domain, the symmetry property can be expressed by the following relation:

$$\tilde{G}\big(k_x, k_y, z|z'\big) = \tilde{G}\big(-k_x, -k_y, z'|z\big) \qquad (26)$$

By expressing all the electromagnetics quantities as a unique function of the normal components of the electric and magnetic fields and of their normal derivatives, and by using the reciprocity theorem, the symmetrical character of the Green's functions can be determined. In this way, we can prove, by careful inspection of eqs. (8), (12), and (14) that $\tilde{G}_A^{xx}$, $\tilde{G}_A^{yy}$, and $\tilde{G}_V^{(DEX)}$ are symmetric, while $\tilde{G}_A^{zx}$, $\tilde{G}_A^{zy}$, $\tilde{G}_A^{zz}$, and $\tilde{G}_V^{(DEZ)}$ are not. Moreover, the application of the reciprocity theorem to the new dyadic $\overline{\overline{\Gamma}}_A$ [eq. (17)] shows that $\overline{\overline{\Gamma}}_A$ itself is reciprocal; that is:

$$\tilde{\Gamma}_A^{uz}(\mathbf{r} \mid \mathbf{r}') = \tilde{\Gamma}_A^{uz}(\mathbf{r}' \mid \mathbf{r}) = \tilde{G}_A^{zu}(\mathbf{r}' \mid \mathbf{r}); \quad u = x, y \qquad (27)$$

METHOD OF MOMENTS

The well known MoM has been selected to transform the MPIE into an algebraic matrix equation of the form $A\mathbf{x} = \mathbf{b}$, which can be solved on a computer. Here, all the metallic surfaces, horizontal and vertical, are meshed with rectangular

cells. Following a well-established approach [3], every couple of cells is filled with a rooftop basis function, and line-matching (razor test functions) is applied between the center of contiguous cells with these assumptions. It has been observed that, for 2-D problems, the Galerkin method is not the only one to guarantee a symmetric matrix of moments. Indeed, the line-matching procedure (razor test), which has been successfully applied to many microstrip problems [3, 4, 7, 17], leads a symmetric matrix. This lucky result disappears if line matching is applied to 3-D planar problems and only a Galerkin method would keep the matrix symmetrical. The mesh associated with a typical 3-D planar structure (short-circuited microstrip antenna) is presented in Figure 6. Now, the matrix A can be divided formally into the form of Figure 7. For instance, the $(A|E)$ block includes the effect of z-oriented vertical source cells on x-oriented horizontal observer cells. Another problem when dealing with 3-D planar structures is the need for using basis and test functions defined on bend surfaces like the broken rooftop (type C of Fig. 6). We propose for these functions an alternative to eqs. (18) and (19) for the calculation of the scattered field. Let us consider that $\mathbf{J}_s = \mathbf{J}_{st}$ in the horizontal (tangential) part of the rooftop and $\mathbf{J}_s = \mathbf{J}_{sn}$ in the vertical (normal) part. We introduce, as a definition, the fact that the components of these currents normal to the boundaries of their definition domain do vanish. This is always possible by including discontinuities in the definition of the current. For instance, we could have:

$$\mathbf{J}_{st} = \begin{cases} x\hat{\mathbf{e}}_x & 0 \le x < 1 \\ 0 & x = 1 \end{cases} \tag{29}$$

The surface charge distributions can be defined as:

$$q_{s(t,n)} = -\nabla' \cdot \mathbf{J}_{s(t,n)}/j\omega \tag{30}$$

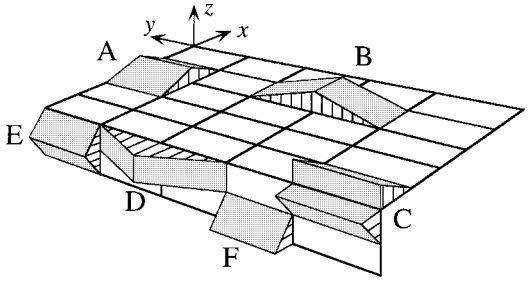

Figure 6. A possible rectangular mesh showing the different types of basis rooftop functions involved in a bent structure.

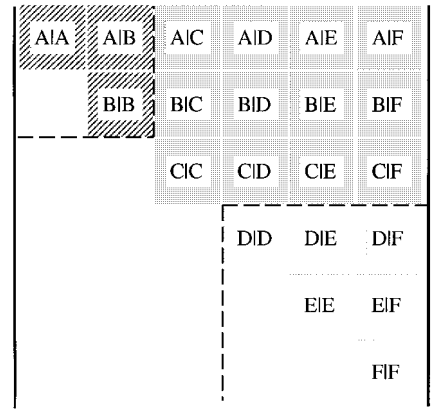

Figure 7. Structure of the moment matrix corresponding to the mesh in Figure 6.

These distributions include Dirac deltas if the corresponding current are discontinuous, like in a broken rooftop. Applying now a formal integration by parts with respect to the coordinate z', we can show easily that eq. (19) becomes:

$$\begin{cases} \mathbf{A}(\mathbf{r} \mid \mathbf{r}') = \displaystyle\int_S \overline{\overline{\mathbf{G}}}_A(\mathbf{r} \mid \mathbf{r}') \cdot (\mathbf{J}_{st}(\mathbf{r}') + \mathbf{J}_{st}(\mathbf{r}'))\, ds' \\ V(\mathbf{r} \mid \mathbf{r}') = \displaystyle\int_{S_t} G_V^t(\mathbf{r} \mid \mathbf{r}') q_{st}(\mathbf{r}')\, ds' \\ \qquad\qquad + \displaystyle\int_{S_n} G_V^n(\mathbf{r} \mid \mathbf{r}') q_{sn}(\mathbf{r}')\, ds' \end{cases} \tag{31}$$

This is a very practical form for construction of a MPIE. In the case of the broken rooftop of Figure 6 (type C), q_{st} will include a positive Dirac delta and q_{sn} a negative one, both defined on the common edge. This is the mathematical description of a line charge distribution ρ_l. Therefore, we write:

$$\begin{aligned} q_{st} &= \hat{q}_{st} + \rho_l \delta \\ q_{sn} &= \hat{q}_{sn} - \rho_l \delta \end{aligned} \tag{32}$$

where the circumflex indicates a regular bounded part. Finally, the scalar potential in eq. (20) becomes:

$$V = \int_{S_t} G_V^t q_{st}\, ds' + \int_{S_n} G_V^n q_{sn}\, ds' + \int_L (G_V^t - G_V^n)\rho_l\, dl' \tag{33}$$

where L is the common edge of S_t and S_n. It is worthwhile to point out that the "difference Green's function," $G_V^t - G_V^n$, vanishes when the source–observer distance goes to zero. Hence, eq. (33) is very convenient from a numerical point of view. Indeed, the contribution of the line charge to the total scalar potential is very frequently small.

RESULTS

To demonstrate the validity of this formulation, the example of a short-circuited microstrip patch antenna has been selected first. The short-circuited condition is achieved by bending one of the patch's edges and connecting it to the ground plane rather than using several via-holes (Fig. 8). The antenna is realized on Duroid 5870 substrate. The relative permittivity is 2.33, the loss tangent 0.0012, and the thickness 1.57 mm. The ground plane and the patch are etched; the vertical metallization has a thickness of 0.1 mm and is soldered to both the ground plane and the patch. The feed for this and the subsequent antennas is a coaxial connector. Although it could be modeled with our technique with the same accuracy as the short-circuit itself, experience shows that the simpler model proposed in ref. 3 (unit vertical current) suffices for accurate predictions in our case. For the analysis, the horizontal patch is divided into 5×5 cells and the vertical metallization into 5×2 cells. Figure 9 shows the input impedance of the short-circuited antenna between 2.6 and 2.95 GHz; each step is 0.05 GHz. The continuous curve represents measurements performed with the HP 8510C network analyzer, whereas the dotted curve shows the theoretical predictions. The simulations agree well with the measurements, particularly concerning the central frequency predictions. However, the simulated curve is systematically inside the measured results. This means that the theoretical predicted *quality factor* is slightly lower than the measured value. This could be due to small differences between the actual loss tangent values and the ones used in the simulation.

The second structure is the two-layered antenna depicted in Figure 10. In this antenna, the patch has two parts, each one at a different level and connected by a continuous vertical metallic wall. The antenna is built using two different substrates. The lower one (RO 3003) has a relative permittivity of 3, a loss tangent of 0.0013, and a thickness of 1.57 mm. It supports the ground plane and an etched patch. The upper substrate is the same as the one used for the short-circuited antenna. Both substrates are glued together with a bonding film of permittivity of 2.28, a loss tangent of 0.003, and an estimated thickness of 38 μm. For the analysis, the two horizontal patches are divided into 12×12 cells and the vertical element into 12×3 cells. Figures 11 and 12 show the input impedance of this antenna between 1.9 and 2.3 GHz, respectively, between 2.4 and 3.0 GHz; each step is 0.025 GHz. Again, the theoretical results agree well with the measurements. Note here the systematic small shift in frequency.

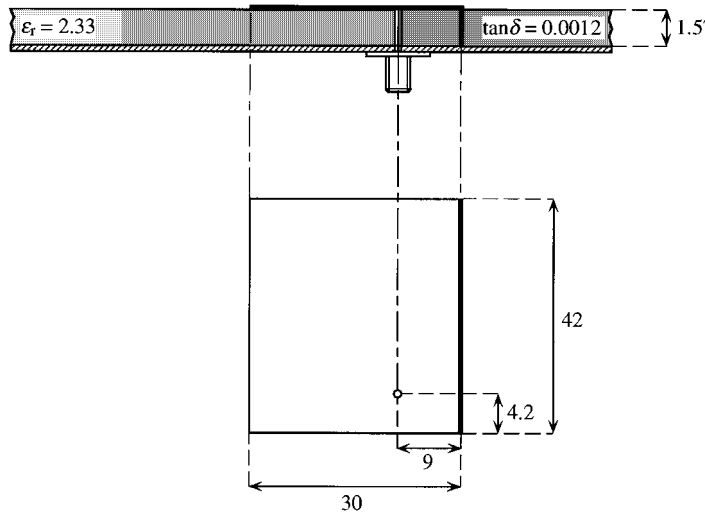

Figure 8. The short-circuited microstrip antenna. All the dimensions are in millimeters.

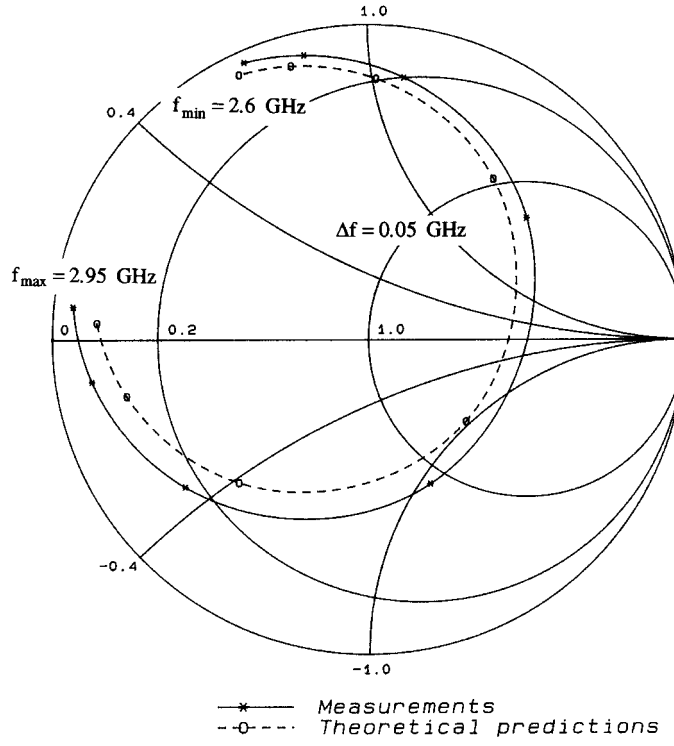

Figure 9. The input impedance of the short-circuited microstrip antenna between 2.6 and 2.95 GHz (step = 0.05 GHz).

This could be due to the bonding film which has been ignored in the simulation procedure. It must also be pointed out that while the measured behavior is very well predicted in the 1.9–2.3-GHz band, results are less accurate in the higher 2.4–3.0-GHz band. This is essentially due to the complex response of the antenna at these frequencies (loop in the impedance locus at low level), but the qualitative behavior is well predicted.

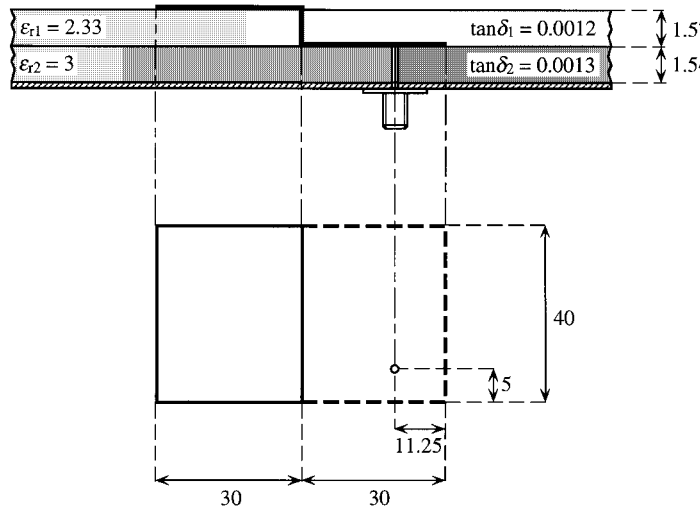

Figure 10. The two-layer microstrip patch antenna. All the dimensions are in millimeters.

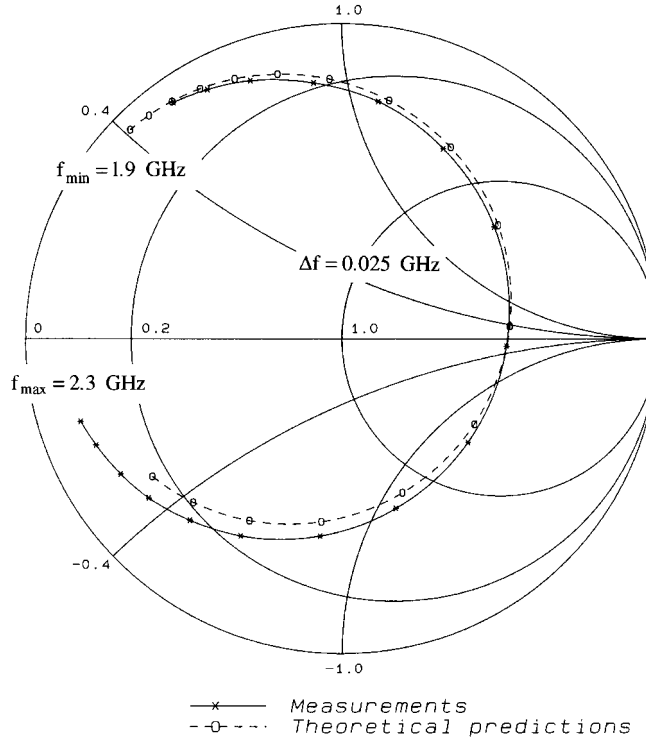

Figure 11. The input impedance of the two-layer microstrip patch antenna between 1.9 and 2.3 GHz (step = 0.025 GHz).

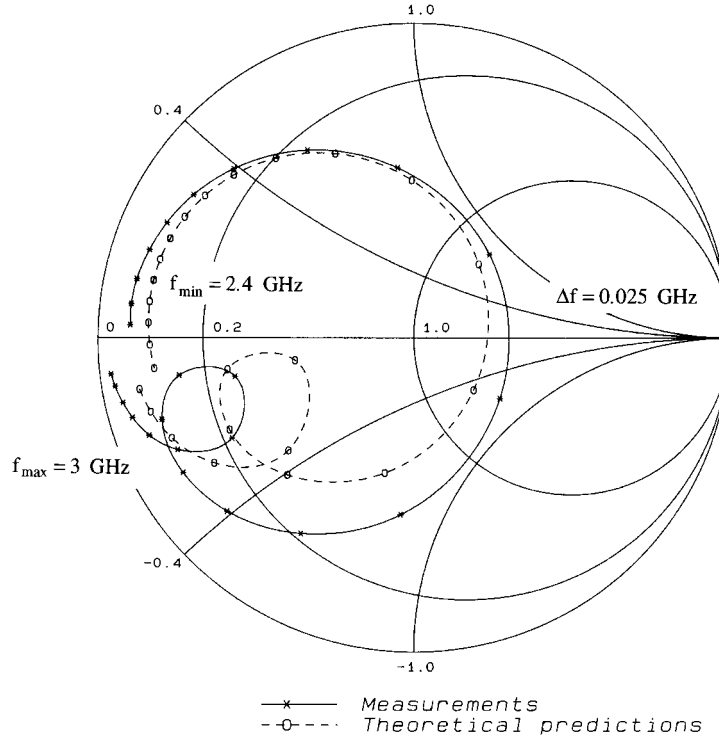

Figure 12. The input impedance of the two-layer microstrip patch antenna between 2.4 and 3.0 GHz (step = 0.025 GHz).

Both antennas must be considered as test structures to validate theory; they have not been produced for any specific application.

CONCLUSIONS

Several 3-D planar antennas including vertical currents in multilayered substrates have been analyzed using an integral equation technique. A good correspondence for the input impedance has been achieved in all cases. This demonstrates that an integral equation approach is a useful tool to study such structures, provided that care is taken in the choice and implementation of basis and test functions. In particular, the moment's matrix will include "hybrid" terms arising from currents and fields which combine both horizontal and vertical components. A possible way to deal with these terms is to add a line charge in edges acting through a difference scalar Green's function. As expected, the line-matching procedure gives rise to a nonsymmetric matrix. The issues of symmetrizing the matrix or using a Galerkin technique should be further investigated. Also the behaviors of the Green's functions on the ground plane and at the interfaces have been studied in detail; then, an interpolation procedure has been developed to take care of interactions where source and observer might be at an arbitrary height above the ground. The good agreement between the measurements and the theoretical results for the antennas under study validates the different numerical algorithms proposed in this work.

ACKNOWLEDGMENTS

The authors thank Mr. M. Hermanjat of the electronics workshop of the Electrical Department of the EPFL for the very precise and careful realization of the various antennas, and our colleague Mr. J. F. Zurcher for his enthusiastic and generous support.

REFERENCES

1. J. M. Baracco, P. Brachat, and J. L. Guiraud, "Shielded Microstrip Subarrays with Large Bandwidth and Low Level of Cross Polarization," *Proceedings of the Journées Internationales de Nice sur les Antennes* (JINA '92), Nice, France, November 1992, pp. 389–392.
2. D. H. Schaubert, "Multilayer and Parasitic Configurations," in J. R. James and P. S. Hall (eds.), *Handbook of Microstrip Antennas*. Peter Peregrinus, London, 1989.
3. J. R. Mosig, R. C. Hall, and F. E. Gardiol, "Numerical Analysis of Microstrip Patch Antennas," in J. R. James and P. S. Hall (eds.), *Handbook of Microstrip Antennas*. Peter Peregrinus, London, 1989.
4. J. R. Mosig, "Integral Equation Techniques," in T. Itoh (ed.), *Numerical Techniques for Microwave and Millimeter-Wave Passive Structures*. John Wiley & Sons, New York, 1989.
5. D. L. Wu, D. C. Chang, and J. X. Zheng, "A Review of Electromagnetic Properties and the Full Wave Analysis of Guiding Structures in MMIC," *Proc. IEEE* (special issue on Electromagnetics), Vol. 79, 1991, pp. 1529–1537.
6. K. A. Michalski, "The mixed-potential electric field integral equation for objects in layered media," *Arch. Elek. Übertragung*, Vol. 39, Sept/Oct. 1985, pp. 317–322.
7. R. C. Hall and J. R. Mosig, "The Analysis of coaxially Fed Microstrip Antennas with Electrically Thick Substrates," *Electromagnetics*, Vol. 9, 1989, pp. 367–384.
8. K. A. Michalski and J. R. Mosig, "Discrete Complex Image MPIE Analysis of Coax-Fed Coupled Vertical Monopoles in Grounded Dielectric Substrate: Two Formulations," *IEE Proc. Microwave Ant. Propagat.*, Vol. 142, No. 3, June 1995, pp. 269–274.
9. K. A. Michalski and D. Zheng, "Electromagnetic Scattering and Radiation by Surfaces of Arbitrary Shape in Layered Media, Part I: Theory," *IEEE Trans. AP*, Vol. AP-38, No. 3, 1990, pp. 335–344.
10. K. A. Michalski and D. Zheng, "Electromagnetic Scattering and Radiation by Surfaces of Arbitrary Shape in Layered Media, Part II: Implementation and Results for Contiguous Half-Spaces," *IEEE Trans. AP*, Vol. AP-38, No. 3, 1990, pp. 345–352.
11. K. Hirasawa and M. Haneishi, *Analysis, Design, and Measurement of Small and Low-Profile Antennas*. Artech House, Boston, 1992.
12. G. Di Massa and G. Mazzarella, "Shorted Annular Patch Antenna," *Microwave and Opt. Technol. Lett.*, Vol. 8, No. 4, 1995, pp. 222–226.
13. C. Delaveaud, P. Leveque, and B. Jecko, "New Kind of Microstrip Antenna: the Monopolar Wire-Patch Antenna," *Electron. Lett.*, Vol. 30, No. 1, January 1994, pp. 1–2.
14. A. John and R. H. Jansen, "A Simple New Technique for the Implementation of Vertical Currents into the SDA," *Microwave Opt. Technol. Lett.*, Vol. 7, No. 9, June 1994, pp. 389–392.
15. H. Aroudaki and V. Hansen, "Full-Wave Analysis of Three-Dimensional Microstrip Discontinuities by a New Spectral Domain Approach," *IEEE AP-S*

International Symposium (Seattle, WA), Vol. III, June 1994, pp. 1694–1701.
16. I. P. Theron and J. H. Cloete, "On the Surface Impedance Used to Model the Conductor Losses of Microstrip Structures, *Proc. IEE Part H*, Vol. 142, No. 1, 1995, pp. 35–40.
17. L. Barlatey, H. Smith, and J. R. Mosig, "Printed Radiating Structures and Transitions in Multilayered Substrates," *Int. J. MIMICAE*, Vol. 2, No. 4, 1992, pp. 273–285.
18. R. P. Feynman, R. B. Leighton, and M. Sands, *Lectures on Physics* (Vol. 2), Addison-Wesley, Menlo Park, CA, 1977, pp. 6-4, 6-6.
19. H. Legay, R. Gillard, J. Citerne, and G. Piton, "Via-Hole Effects on Radiation Characteristics of a Patch Microstrip Antenna Coaxially Fed Through the Grond Plane," *Ann. Telecommun.*, Vol. 46, Nos. 7–8, 1991, pp. 367–381.
20. E. H. Newman and D. Forrai, "Scattering from a Microstrip Patch," *IEEE Trans. AP*, Vol. AP-35, No. 3, 1987, pp. 245–251.
21. U. V. Gothelf, "A Computational Model of an Aperture Coupled Microstrip Antenna," PhD Thesis LD 110, Technical University of Denmark, 1994.
22. K. A. Michalski and C. M. Butler, "Evaluation of Sommerfeld Integrals Arising in the Ground Stake Antenna Problem," *IEE Proc.* Vol. 134, Pt. H, No. 1, February 1987, pp. 93–97.
23. G. J. Burke et al., "Computer Modeling of Antennas Near the Ground," *Electromagnetics*, Vol. 1, 1981, pp. 29–49.

BIOGRAPHIES

Philippe Gay-Balmaz was born in Vernayaz, Switzerland. In 1990, he received the electrical engineering degree from the Swiss Federal Institute of Technology at Lausanne (EPFL). Since 1990 he has been a collaborator at the Laboratory of Electromagnetics and Acoustics of the EPFL. From 1991 to 1993 he developed SSFIP antennas. He then began work on his PhD thesis, studying 3-D planar structures in stratified media. He presented his thesis in September 1996.

Juan R. Mosig was born in Cadiz, Spain. He received the electrical engineering degree in 1973 from Universidad Politecnica de Madrid, Spain. In 1976 he joined the Laboratory of Electromagnetics and Acoustics at Ecole Polytechnique Fédérale de Laussane (EPFL), Switzerland, from which he obtained a PhD degree in 1983. Since 1991 he has been an associate professor at the EPFL. In 1984, he was a visiting research associate at Rochester Institute of Technology, Rochester, NY. He has also held scientific appointments at the Universities of Rennes (France), and Nice (France), the Technical University of Denmark, and the University of Colorado, Boulder, CO. Dr. Mosig is the author of four chapters in books on microstrip antennas and circuits. His research interests include electromagnetic theory, numerical methods, and microstrip antennas.

射 频 和 天 线 设 计 培 训 课 程 推 荐

易迪拓培训(www.edatop.com)由数名来自于研发第一线的资深工程师发起成立，致力并专注于微波、射频、天线设计研发人才的培养；我们于 2006 年整合合并微波 EDA 网(www.mweda.com)，现已发展成为国内最大的微波射频和天线设计人才培养基地，成功推出多套微波射频以及天线设计经典培训课程和 ADS、HFSS 等专业软件使用培训课程，广受客户好评；并先后与人民邮电出版社、电子工业出版社合作出版了多本专业图书，帮助数万名工程师提升了专业技术能力。客户遍布中兴通讯、研通高频、埃威航电、国人通信等多家国内知名公司，以及台湾工业技术研究院、永业科技、全一电子等多家台湾地区企业。

易迪拓培训课程列表：http://www.edatop.com/peixun/rfe/129.html

射频工程师养成培训课程套装

该套装精选了射频专业基础培训课程、射频仿真设计培训课程和射频电路测量培训课程三个类别共 30 门视频培训课程和 3 本图书教材；旨在引领学员全面学习一个射频工程师需要熟悉、理解和掌握的专业知识和研发设计能力。通过套装的学习，能够让学员完全达到和胜任一个合格的射频工程师的要求…

课程网址：http://www.edatop.com/peixun/rfe/110.html

ADS 学习培训课程套装

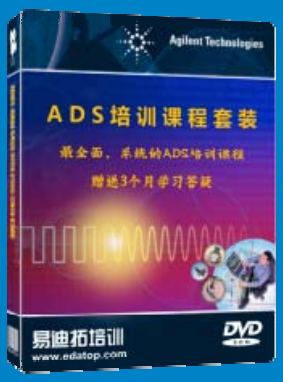

该套装是迄今国内最全面、最权威的 ADS 培训教程，共包含 10 门 ADS 学习培训课程。课程是由具有多年 ADS 使用经验的微波射频与通信系统设计领域资深专家讲解，并多结合设计实例，由浅入深、详细而又全面地讲解了 ADS 在微波射频电路设计、通信系统设计和电磁仿真设计方面的内容。能让您在最短的时间内学会使用 ADS，迅速提升个人技术能力，把 ADS 真正应用到实际研发工作中去，成为 ADS 设计专家...

课程网址： http://www.edatop.com/peixun/ads/13.html

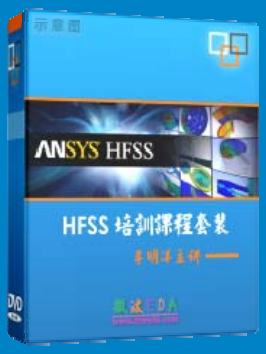

HFSS 学习培训课程套装

该套课程套装包含了本站全部 HFSS 培训课程，是迄今国内最全面、最专业的 HFSS 培训教程套装，可以帮助您从零开始，全面深入学习 HFSS 的各项功能和在多个方面的工程应用。购买套装，更可超值赠送 3 个月免费学习答疑，随时解答您学习过程中遇到的棘手问题，让您的 HFSS 学习更加轻松顺畅…

课程网址：http://www.edatop.com/peixun/hfss/11.html

CST 学习培训课程套装

该培训套装由易迪拓培训联合微波 EDA 网共同推出，是最全面、系统、专业的 CST 微波工作室培训课程套装，所有课程都由经验丰富的专家授课，视频教学，可以帮助您从零开始，全面系统地学习 CST 微波工作的各项功能及其在微波射频、天线设计等领域的设计应用。且购买该套装，还可超值赠送 3 个月免费学习答疑…

课程网址：http://www.edatop.com/peixun/cst/24.html

HFSS 天线设计培训课程套装

套装包含 6 门视频课程和 1 本图书，课程从基础讲起，内容由浅入深，理论介绍和实际操作讲解相结合，全面系统的讲解了 HFSS 天线设计的全过程。是国内最全面、最专业的 HFSS 天线设计课程，可以帮助您快速学习掌握如何使用 HFSS 设计天线，让天线设计不再难…

课程网址：http://www.edatop.com/peixun/hfss/122.html

13.56MHz NFC/RFID 线圈天线设计培训课程套装

套装包含 4 门视频培训课程，培训将 13.56MHz 线圈天线设计原理和仿真设计实践相结合，全面系统地讲解了 13.56MHz 线圈天线的工作原理、设计方法、设计考量以及使用 HFSS 和 CST 仿真分析线圈天线的具体操作，同时还介绍了 13.56MHz 线圈天线匹配电路的设计和调试。通过该套课程的学习，可以帮助您快速学习掌握 13.56MHz 线圈天线及其匹配电路的原理、设计和调试…

详情浏览：http://www.edatop.com/peixun/antenna/116.html

我们的课程优势：

※ 成立于 2004 年，10 多年丰富的行业经验，

※ 一直致力并专注于微波射频和天线设计工程师的培养，更了解该行业对人才的要求

※ 经验丰富的一线资深工程师讲授，结合实际工程案例，直观、实用、易学

联系我们：

※ 易迪拓培训官网：http://www.edatop.com

※ 微波 EDA 网：http://www.mweda.com

※ 官方淘宝店：http://shop36920890.taobao.com